

CHARACTERISATION OF OPTICAL VORTICES

Guy Leckenby

Supervisor: Benjamin Buchler

PhB Advanced Studies Course, Department of Quantum Science, RSPE
The Australian National University, Canberra, ACT 2611, Australia

November 11, 2016[†]

ABSTRACT

Optical vortices are found everywhere three plane waves intersect and are hence of crucial significance to our understanding of light. In this report, we describe the theoretical origins of optical vortices and demonstrate some of their fundamental properties experimentally. In particular, a spiral phase mirror was used to construct a charge 2 optical vortex which was imaged three dimensionally to analyse the volumetric structure. The charge was determined by using a Michelson interferometer which generated a forked interference pattern. Finally further research is proposed in the form of phase mappings, observing the decay of high charge optical vortices and the three dimensional analysis of optical knots and links.

I. INTRODUCTION

For a phenomena that has only been investigated relatively recently, optical vortices appear with impressive frequency in nature as they can occur whenever three or more light waves interfere. In particular they are points in the interference field characterised by an undefined phase and an associated zero intensity value [1]. The first investigation into the dislocation of wave trains was conducted by Nye & Berry [2] and since then they have garnered extensive theoretical and experimental interest.

Apart from a purely theoretical interest, there have been many applications developed for optical vortices. Carpentier et al. [3] reported on variety of implementations. Vortices can be used as optical tweezers to trap neutral particles by transferring the angular momentum associated with the rotation of the phase [4]. They find use in extrasolar planetary observations using optical vortex coronagraphs by blocking the light from bright stars to increase the contrast in the image [5]. Finally applications in quantum information have been proposed employing the quantised properties of the angular momentum associated with vortices [6].

In this report, we will investigate the theory behind optical vortices and demonstrate the generation and interferometric properties of the vortices.

II. OPTICAL VORTEX THEORY

Optical vortices are characterised by helical wavefronts and the associated helical mode $\psi_m(\mathbf{r})$ (Curtis & Grier, 2003) is given by

$$\psi_m(\mathbf{r}) = R(r, z)e^{-ikz}e^{im\theta}. \quad (1)$$

The phase factor $e^{im\theta}$ describes the phase singularity nature of the vortex where the integer m is the topological charge of the vortex and θ is the azimuthal coordinate about the centre of beam [7]. At $r = 0$, the phase factor becomes undefined and the intensity drops to zero as a result such that $R(0, z) = 0$. The factor m can take on any integer value but as Leach et al. [1] point out, any vortex with $|m| > 1$ is unstable and, in the

presence of an astigmatism, will decompose to form multiple vortices of $m = \pm 1$ upon propagation.

The phase beam propagates in a helical manner, as visualised in Fig. 1, and according to the semiclassical approximation, each photon in this helical mode carries $m\hbar$ orbital angular momentum [8]. Thus the beam can exert a torque proportional to its intensity for particles along the singularity. This orbital angular momentum is a consequence of the azimuthal structure of the optical beam and the associated Poynting also has an azimuthal component resulting in a net flow of energy and momentum around around the vortex [9] as see in Fig. 1. Angular momentum and optical vortices are often studied together however it is important to note that the vortex itself does not carry any momentum (as it has zero intensity) but rather the surrounding phase fronts.

Whilst most optical systems are generally decomposed in terms of Hermite-Gaussian (HG) modes, the natural mode of an optical vortex is a Laguerre-Gaussian (LG) mode [9]. LG modes are characterised by ℓ and p indices which describe the charge of the optical vortex present in LG modes and the number of concentric nodes respectively. Similar to HG modes, LG modes form a complete basis but they are based on vortex structure inherent to Laguerre polynomials. The first few LG

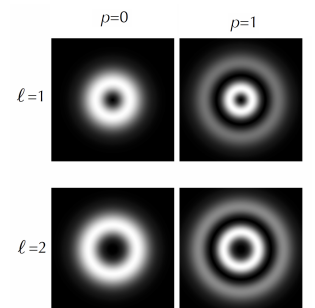
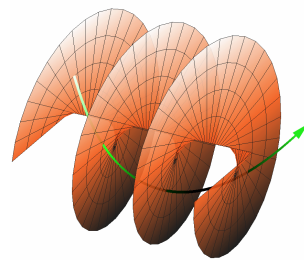
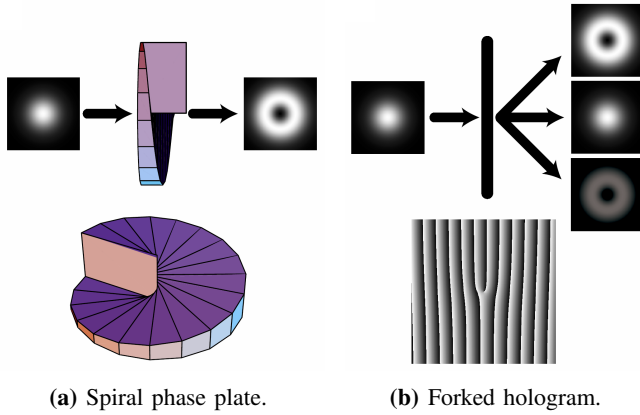


Figure 1: Surface of constant phase around an optical vortex; the Poynting vector is shown in green [9].

Figure 2: The first four Laguerre-Gaussian modes for varying ℓ, p indices [9].

[†]A fortnight extension until the 11th of November was granted by Benjamin Buchler.



(a) Spiral phase plate.

(b) Forked hologram.

Figure 3: Two methods of producing an optical vortex using a machined spiral phase plate or a forked hologram with a blazed diffraction grating (O'Holleran, 2008).

modes are shown in Fig. 2

By far the most common way of generating optical vortices is with a 'forked' hologram where an edge dislocation is added to the centre of a blazed diffraction grating, an example of which is seen in Figure 3b. This will generate a phase modulation of $\text{mod}_{2\pi} |m\lambda\theta/2\pi + \alpha x|$ which generates an optical vortex [9]. These holograms were generalised to be computer generated holograms using spatial light modulators (SLMs). The SLM contains an array of pixels upon which a computer image can be imprinted which defines the spatial variation of phase of intensity of incoming light. The flexibility of SLMs have made them extremely popular for generating vortices.

The precision of SLMs are limited by the pixel size and as a result they cannot generate vortices with charges greater than a couple of hundred. An alternate method, first proposed by Beijersbergen et al. [10], is to machine a spiral phase plate (SPP) as shown in Fig. 3a. Here the required vortex structure is directly mapped onto the structure given by a height of $m\lambda\theta/2\pi$. SPPs can be realised either as a mirror, in which case the light reflects off the spiral plate and the height difference imprints the phase structure on the incoming beam. Alternatively they can also be transparent optical components with a refractive index n where the optical thickness increases with the azimuthal angle such that $\Delta t = \frac{\theta}{2\pi}(n-1)m\lambda$ and hence upon transmission, the beam acquires the required phase term [9]. The advantage of SPPs is that the construction is limited by engineering tolerances rather than pixel size which allows for beams mostly free of astigmatism and the construction of much higher charges given the required engineering prowess. For this experiment, we used mirror SPPs however the precise construction will be described in further detail in the following section.

III. GENERATING VORTEX BEAMS

For this project, precision machined spatial phase mirrors (SPM) were used to produce optical vortices. The SPMs used were those developed by Shen et al. [7] and the precise methodology comprises a significant portion of their paper. In particular, the SPMs are produced by direct machining onto

an aluminium disc using an ultra-high precision single point diamond turning lathe. For the low charge plates considered here, a height of $d(\theta) = m\lambda/4\pi$ was used however a more complicated modular height was used for higher charge plates. Though the machining process does produce some defects, particularly near the centre of the disc, these have negligible impact on the quality of the resulting vortex beam [7], especially for low charge SPMs.

To image the optical vortices, we used the set up pictured in Fig. 4. For a simple optical vortex, the top arm of the interferometer was blocked and the rail track fixed. A neutral density filter was used to ensure the CCD was not overexposed and the beam width was reduced threefold with a lens array to ensure the entire pattern fitted on the CCD array. The beam splitter was adjustably mounted to ensure the TEM₀₀ input beam from the laser was centred on the SPM. The second lens array was included for spatial filtering however this was not used in most measurements as the high spatial frequencies were noise based rather than from imperfections in the SPM.

The beam was then directed to the CCD. The exposure time was manually adjusted such that the brightest features in each

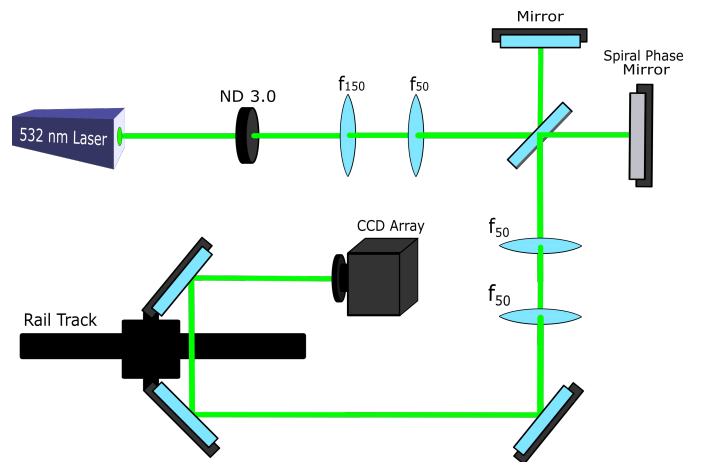


Figure 4: The experimental set up which was used to analyse the various characteristics of optical vortices.

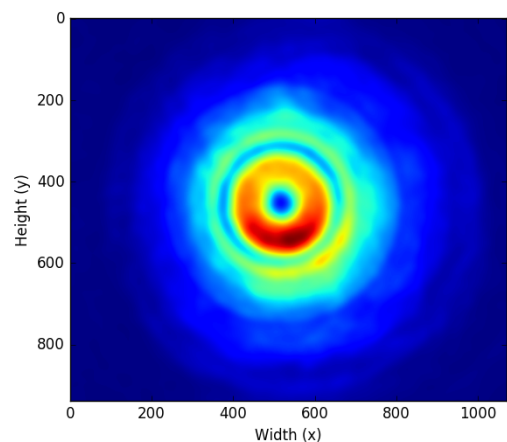


Figure 5: A charge 2 optical vortex after image smoothing.

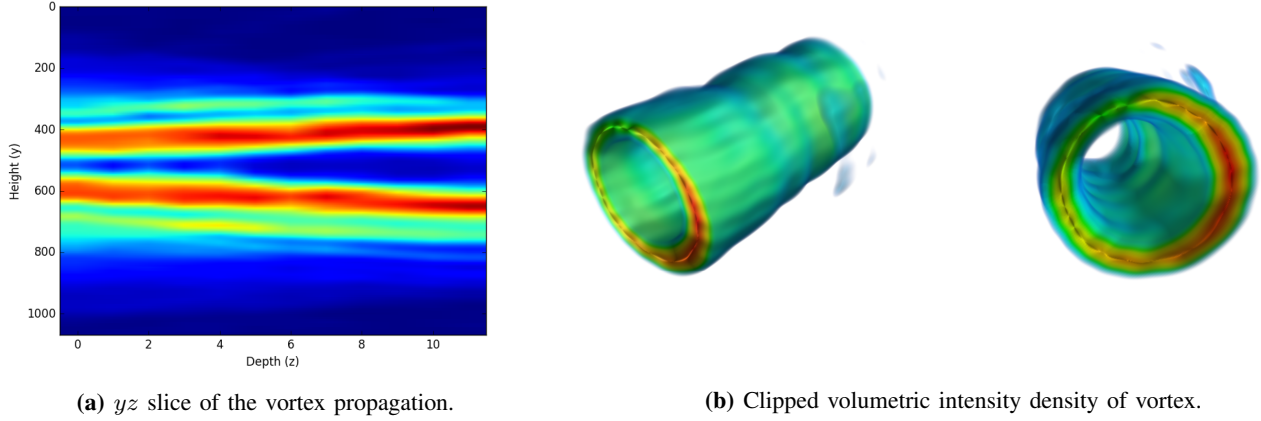


Figure 6: 3D volumetric data from a charge 2 optical vortex. The propagation distance is approximately 55 cm.

image were not overexposed. On top of this, we tried several de-noising algorithms however 12-sigma Gaussian blurring was chosen as most of the high frequency information was noise or diffraction related. A more thorough discussion of the image handling can be found in Appendix A.

An example of the images produced by this method is shown in Fig. 5 where a TEM_{00} input beam is applied to a charge 2 SPM. As predicted, the intensity at the centre of the vortex is zero whilst a bright ring is seen around the beam axis. A second, smaller, outer ring is also seen. We believe that this is generated by an impurity in the LG_0^2 mode due to the presence of the LG_1^1 mode which contains an extra circular node as seen in Fig. 2. This ring was also observed in charge 2 vortices by Carpentier et al. [3]. Whilst vortices are supposed to have cylindrical symmetry, it is clear that the observed vortex does not and is in fact more intense on the lower side of the ring. We believe this was due to alignment issues with the optical system as a whole as the input beam was centred on the SPM for these measurements.

IV. 3D VOLUMETRIC MAPPING

Whilst examining the two dimensional structure of vortices is interesting, it does not reveal everything about the vortices themselves. In fact the structure of vortices in three dimensional space is much more interesting as it can produce much more complicated systems like knots and links. To this end, we used the rail track, pictured in Fig. 4, to map the three dimensional structure of vortex beams by taking slices at various beam lengths and combining them digitally. In particular, for the charge 2 vortex presented, the beam length was increased by sliding the two mirrors backwards on the rail track by 2.5 cm for 12 different image frames. As a 2.5 cm backwards step for the rail track apparatus corresponds to a 5 cm increase in the beam path length, a 55 cm long image of the beam was produced.

Each frame was 12-Sigma Gaussian blurred and centred using the symmetry properties of the vortex. The images were then combined into 3D array which could then be visualised computationally in a number of ways (more information of the computational construction of the 3D array can be found in

Appendix A). In particular, we took a longitudinal slice to see the evolution of the vortex beam which can be seen in Fig. 6a. As evident, the vortex diverges with increasing distance from the vortex plate but the structure is maintained.

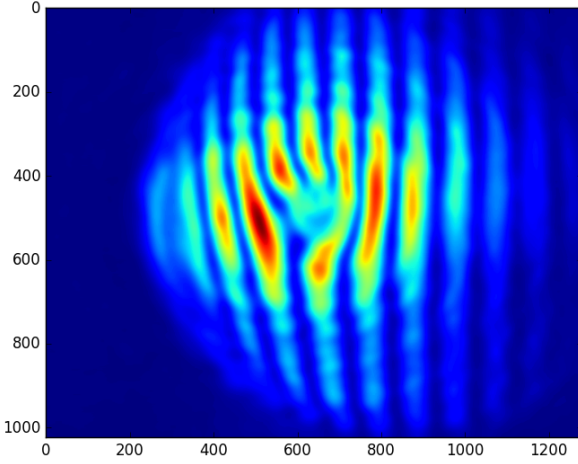
We were also able to produce more interactive images of the 3D array. Fig. 6b shows a volumetric intensity plot which demonstrates the 3D structure of the optical vortex. This plot has been clipped to remove the intensity associated with everything below the 60th percentile. It does however demonstrate the tube-like nature of propagating vortices and, to some extent, the divergence of cylindrical intensity ring.

Whilst we were not able to produce optical knots in this investigation, the capabilities for this 3D volumetric imaging makes visualising them very exciting as we would not only be able to visualise the dark vortex threads themselves but the intensity structures associated. Although they could not be included in a static report, we were also able to construct animations which scan the 3D structure both parallel and perpendicular to the cylindrical axis of symmetry.

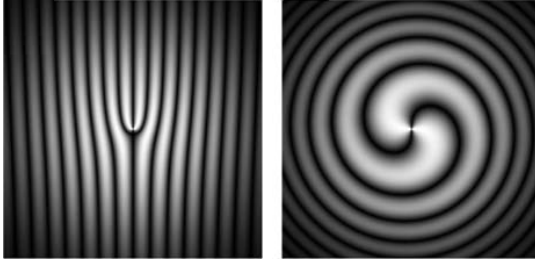
V. INTERFEROMETRIC ANALYSIS

Intensity analysis can demonstrate many properties of optical vortices however they are fundamentally a phase based phenomena and hence we need to turn to interferometric measurements. Phase is a purely relative concept and to make any phase measurements, you need to introduce an interferometer. In particular, a simple Michelson interferometer was introduced as seen in Fig. 4. Because the input beam needs to be centred on the SPM, the SPM was placed on the transmitted beam and both the beam splitter and ordinary mirror were placed on adjustable mounts such that the interferometer could be aligned. This was then used to make several different phase measurements to infer properties of optical vortices.

Since vortices of varying charge do not have noticeably different intensity profiles, you can utilise interference with a reference beam to determine the charge of the vortex. This is seen in Fig. 7 where the reference beam has been slightly tilted horizontally such that the overlapping beams have slightly different wave-vectors \mathbf{k} . Fig. 7b is the theoretical formulation of what these interference patterns will look like assuming the



(a) Observed planar phase interference pattern for charge 2 vortex.



(b) Theoretical interference patterns for planar (left) and spherical (right) phase provided by Carpentier et al. (2008).

Figure 7: Interference patterns produced by slightly tilting the reference can reveal the charge of an optical vortex, in this case a charge 2 vortex.

reference beam has planar and spherical phase respectively. In the planar case, which is the form observed experimentally in Fig. 7a, the parallel interference lines converge at the optical vortex where $m2\pi$ units of phase are absorbed. In this case, it can be seen that two interference lines are absorbed and thus we conclude that the charge of the vortex is $m = 2$. Unfortunately, the experimental image is marred by a defect precisely at the optical vortex which prevents us from seeing the recombination of the interference lines. The exact cause of this defect was not investigated however the general principles remain clear.

Aligning the beams directly produces a slightly different interference pattern. Given that the incoming beam was Gaussian and the vortex beam has a phase term of $e^{im\theta}$, there are m points where the two beams differ by π and total destructive interference occurs. The perfect example of this is seen in Fig. 8a which was a result determined by Carpentier et al. [3] which clearly shows the two destructive dots predicted. Note that in this case, the charge 2 vortex has decayed into 2 charge 1 vortices when the initial vortex is made to copropagate with the reference beam. When we tried to replicate a similar image, the result was less than successful as seen in Fig. 8b. A slight circular interference pattern can be seen and thus it appears that there was a slight curvature difference between the reference and vortex beam. If this curvature difference could

be corrected, then the desired pattern should emerge.

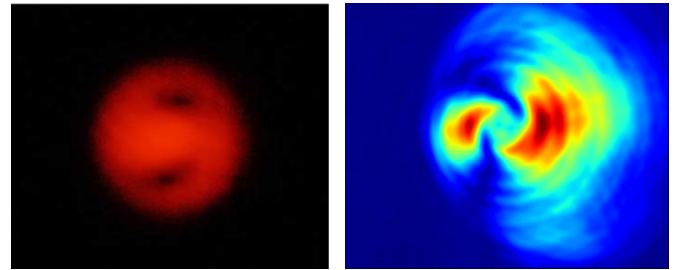
O'Holleran [9] demonstrated that the reference beam can also be used to create phase maps of the vortex itself. In particular, the interference pattern will be altered when the relative phase of the reference beam is changed by changing the arm length of the interferometer. By assigning each pixel an intensity value for each relative phase measurement and varying the phase over an entire 2π phase evolution, the intensity of the pixel can be linked to the relative phase and thus a phase map produced. Whilst very useful for determining precise vortex locations and phase structure, this method is quite hard to implement and we were unable to replicate it due to time pressures. For future investigations however, this would be a promising next step to analysing vortex systems.

VI. FUTURE INVESTIGATIONS

Whilst we were able to observe many of the important properties of optical vortices, there were several phenomena mentioned in section II that we did not have the time to observe. It was predicted that due to the presence of astigmatism in the beam, high charge vortices will decay into single charge vortices. whilst this was unable to be achieved in a 3D volumetric mapping, if the phase maps (described above) could be produced over the 3D volume, the position of the vortices could be tracked directly. This could also be achieved by getting the interference pattern in Fig. 8 to work effectively and observing the propagation.

In this project, we only worked with a charge 2 vortex. It would be instructive to work with higher charges and investigate the propagation and interference patterns produced. Higher charges are more unstable and hence decay faster. Observing this decay chain via 3D phase mapping and the interaction of interference patterns for multiple copropagating high charge vortices would be challenging and illuminating in regards to the additive properties and interactions of optical vortices.

In addition to simple propagation, optical vortices can also be used to produce static knots and links of dark vortex lines in light waves. This was theoretically predicted by Berry & Dennis [11] and was realised experimentally by Leach et al. [1] where they were able to construct temporally stable knots and links. SPMs can theoretically be used to to produce arbitrary



(a) Results from Carpentier et al. (b) Our observation of aligned (2008) demonstrating two points interference although the curvature of destructive interference. of the beams vary.

Figure 8: Aligning the interference beams should produce two points of destructive interference in the following interference pattern.

wavefronts by a finite sequence of phase modulation and Fourier transformations [7]. Hence, given the appropriate theoretical templates, any interesting wavefronts could be machined to high precision. This can be used to construct complex features like optical knots and particle traps from a single TEM₀₀ beam. Whilst constructing the SPM templates is beyond the scope of this report, our set up is capable of imaging such vortices.

There are other systems which produce optical vortices. O'Holleran [9] reported on an analysis of the umbilic diffraction catastrophe. This is an interference pattern produced by diffraction through a bulged triangular lens, most easily constructed from filling a triangular aperture with a drop of water. The following diffraction pattern contains both vortex loops and lines separated into two distinct regimes. This topological structure provides extensive information on 4- and 3-wave interference and would provide deep insights into the presence of optical vortices in nature.

VII. CONCLUSION

In this report we have investigated some of the theoretical properties of optical vortices and realised those predictions experimentally. In particular, optical vortices have been described as light beams with helical wavefronts associated with an azimuthal phase component of $e^{im\theta}$ such that a phase singularity is generated at the centre of the beam with a corresponding zero intensity. Several methods of generating optical vortices were suggested however spiral phase mirrors were chosen due to their high precision. An optical vortex of charge two was then imaged and the bright ring with zero intensity at the centre was observed. A 3D volumetric density image of this vortex was then constructed by combining multiple images taken at increasing distances from the phase mirror. Finally, a Michelson interferometer was used to observe the diffraction pattern produced by tilting a planar phase reference beam which

showed the convergence of two interference lines at the vortex demonstrating the vortex was indeed charge two. A method of producing phase maps was proposed to more effectively track vortex propagation and future work was suggested in characterising the decay of higher charge vortices and imaging optical knots. Thus we have demonstrated experimentally many of the characteristics that make optical vortices appealing for multiple applications.

REFERENCES

- [1] Leach, J., Dennis, M.R., Courtial, J., & Padgett, M.J. 2005. 'Vortex knots in light,' *New Journal of Physics*, **7**, 55, doi:10.1088/1367-2630/7/1/055.
- [2] Nye, J.F. & Berry, M.V. 1973. 'Dislocations in wave trains,' *Proceedings of the Royal Society of London A*, **336**, 165-190; doi: 10.1098/rspa.1974.0012.
- [3] Carpentier, A.V., Michinel, H., Salgueiro, J.R., & Olivieri, D. 2008. 'Making optical vortices with computer-generated holograms,' *American Journal of Physics*, **76**, 916; doi: 10.1119/1.2955792.
- [4] Gahagan, K.T., & Swartzlander, G.A. 1996. 'Optical vortex trapping of particles,' *Optics Letters*, **21**, 8279; doi: 10.1364/OL.21.000827.
- [5] Foo, G., Palacios, D.M., & Swartzlander, G.A. 2005. 'Optical vortex coronagraph,' *Optics Letters*, **30**, 330810; doi: 10.1364/OL.30.003308.
- [6] Mair, A., Vaziri, A., Welhs, G., & Zeilinger, A. 2001. 'Entanglement of the orbital angular momentum states of photons,' *Nature* **412**, 3136; doi: 10.1038/35085529.
- [7] Shen, Y., Campbell, G.T., Hage, B., Zou, H., Buchler, B.C., & Lam, P.K. 2013. 'Generation and interferometric analysis of high charge optical vortices,' *Journal of Optics*, **15**, 044005; doi: 10.1088/2040-8978/15/4/044005.
- [8] Curtis, J.E. & Grier, D.G. 2003. 'Structure of Optical Vortices,' *Physical Review Letters*, **90**, 133901; doi: 10.1103/PhysRevLett.90.133901.
- [9] O'Holleran, K. 2008. *Fractality and topology of optical singularities*. Doctoral thesis, University of Glasgow, Glasgow.
- [10] Beijersbergen, M.W., Coerwinkel, R.P.C., Kristensen, M., & Woerdman, J.P. 1994. 'Helical-wavefront laser beams produced with a spiral phaseplate,' *Optics Communications*, **112**, 321-7; doi: 10.1016/0030-4018(94)90638-6.
- [11] Berry, M.V. & Dennis, M.R. 2001. 'Knotted and linked phase singularities in monochromatic waves,' *Proceeding of the Royal Society of London A*, **457**, 2251-63; doi: 10.1098/rspa.2001.0826.

APPENDIX A: CONSTRUCTING A 3D INTENSITY ARRAY WITH PYTHON

One of the most challenging aspects of this project was constructing the 3D intensity array from the snapshots imaged. In this appendix, we will present the code used to do this and explain the motivation behind some of our choices.

The first step was choosing how to denoise the images. In particular, there was both background noise associated with light from the laboratory and high frequencies introduced by defects in the optical system. To remove the statistical variation from the background noise, a Rudin-Osher-Fatemi total variation denoising algorithm was implemented as ROF denoising preserves structure of the image whilst smoothing the micro-variations. However, as seen in Fig. 9b, it was found that ROF denoising maintained too many of the high spatial components and thus was ineffective in denoising the image. Instead we used the `scipy` Gaussian filter to apply a 12-sigma Gaussian blur. This produced the intensity profiles seen in Fig. 9a which are much smoother whilst still maintaining the broad structure of the optical vortex. After this the background level was removed by subtracting the average intensity value of $4\ 50 \times 50$ squares from each corner of the image.

Due to imperfections in the optical set up, each image was centred slightly differently. It was important to centre the images on the vortex itself otherwise the various components wouldn't match up when combined. The program was initially tested on a Gaussian beam after a lens and hence centring the beam on the brightest pixel was a good proxy for the centre of the beam line. However the intensity of the beam for an optical vortex is zero by definition on the centre of the beam line. Thus the centre was instead determined by an intensity weighted average over all the pixels. Since the vortex was cylindrically symmetric along the beam axis, this weighted average gave the centre of the vortex. Each image was cropped such that the volume was rectangular. Finally the image was combined into the desired 3D array which was saved externally using `h5py`.

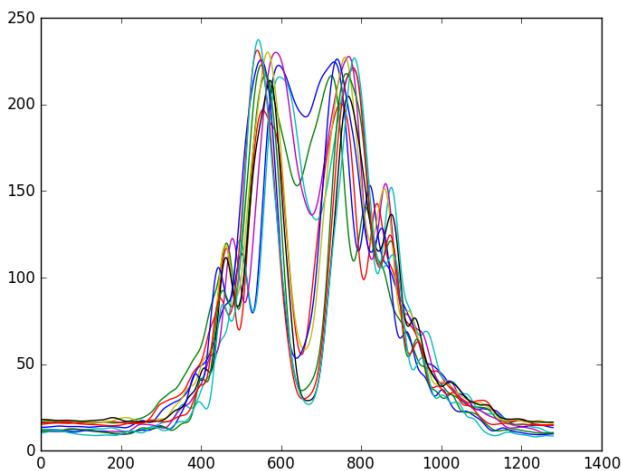
The code which achieved this is presented below:

```
import numpy as np
from PIL import Image
import os
import scipy.ndimage.filters

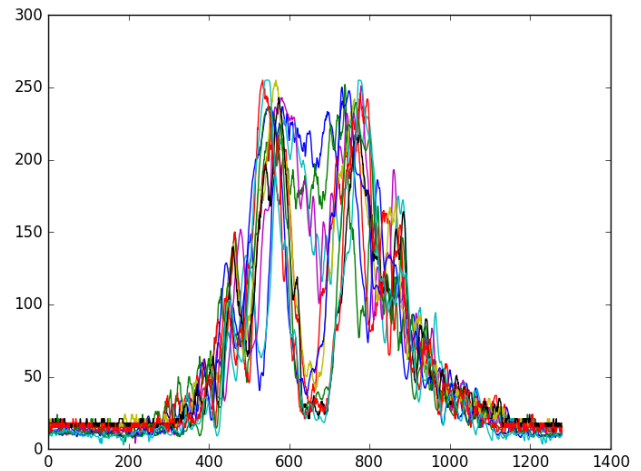
def createArray(imfold, sta, end, inv):
    ''' This script takes raw bitmap images, converts them to numpy arrays, gaussian filters
        them, subtracts the mean background noise level and crops and centres the images into
        an array.
    Inputs: 'imfold' - string specifying the folder containing the CCD images.
           'sta, end, int' - integers determining the separation naming convention.
    Outputs: a 3-dimensional numpy array of floats acting as a 3D beam profile. '''

    filist, cenlist, imlist, arlist = [], [], [], []
    maxx, maxy = -1, -1

    # Creates a list of file names to be examined.
    for i in range(sta, end, inv):
        filist.append(os.path.abspath('CCD Images/' + imfold + '/D+' + str(i) + '.bmp'))
```



(a) A 12-sigma Gaussian filter.



(b) ROF denoising filter.

Figure 9: Above are several intensity profiles for x slices of an observed optical vortex for both Gaussian filtering and ROF denoising.

```

for i in filist:
    with Image.open(i).convert('L') as im:
        # Converts image to array, gaussian filters the image and subtracts background noise.
        imar = np.array(im, 'f')
        imarf = scipy.ndimage.filters.gaussian_filter(imar, 12)
        (dimx, dimy) = imarf.shape
        bkgrnoise = np.mean([imar[0:50, 0:50], imar[0:50, dimy - 50:dimy], imar[dimx -
            50:dimx, dimy - 50:dimy], imar[dimx - 50:dimx, 0:50]])
        imarf = imarf - bkgrnoise
        imlist.append(imarf)

        # Calculcates centre of interference pattern
        avgpix = [0, 0]
        for m in range(dimx):
            for n in range(dimy):
                avgpix = [avgpix[0] + int(imarf[m, n]) * m, avgpix[1] + int(imarf[m, n]) * n]
        finavgpix = [avgpix[0] / (m * n * imarf.mean()), avgpix[1] / (m * n * imarf.mean())]
        cenlist.append(finavgpix)

        # Iteratively checks for most off centre image.
        if abs(finavgpix[0] - 512) > maxx:
            maxx = abs(finavgpix[0] - 512)
        if abs(finavgpix[1] - 620) > maxy:
            maxy = abs(finavgpix[1] - 620)

imlist = np.stack(imlist)
maxwidth, maxheight = int(512 - maxx - 1), int(620 - maxy - 1)

# Crops images and forms them into an 3-dimensional array.
for i in range(len(filist)):
    cenx, ceny = cenlist[i]
    cenim = imlist[i, int(cenx) - maxwidth:int(cenx) + maxwidth, int(ceny) -
        maxheight:int(ceny) + maxheight]
    arrlist.append(cenim)

# Returns the 3-dimensional beam image.
return np.stack(arrlist)

```

The 3D array constructed will have dimensions of pixels squared by the number of images. As the number of images is usually two orders of magnitude smaller than the number of pixels in each image, the 3D array often needs to be interpolated along the z axis. To do this, `scipy.ndimage.interpolation.zoom` was used which does linear interpolation of arrays. From the 3D array, any image or slice can be taken using standard python graphics packages. To produce the volumetric density plots, `Mayavi` was used, in particular `mlab.pipeline.volume(mlab.pipeline.scalar_field(array))`.